Modelling Drag Forces on a Wheelchair Racing Simulator

Ateayeh Bayat[1,3] and Félix Chénier[1,2,3]
[1]Department of Systems Engineering, École de Technologie Supérieure (ÉTS), Montreal, Canada
[2]Department of Physical Activity Sciences, Université du Québec à Montréal (UQAM), Canada
[3]Centre for Interdisciplinary Research in Rehabilitation of Greater Montreal (CRIR), Canada

Keywords: Racing Wheelchair, Simulator, Dynamic Model, Drag Force.

Abstract: A racing wheelchair simulator is a stationary device that allows para-athletes to train inside, in different simulated conditions (e.g., rolling resistance, wind). Apart from improving performance during training sessions, it also allows researchers to study the biomechanics of the propulsion in a laboratory, which is important because wheelchair racing can cause musculoskeletal disorders and pain in athletes. For these reasons, the realism of these simulators is paramount, and having a model that reproduces a non-linear relationship between drag force, wheeling speed and wind speed is one of the criteria for achieving this realism. In this work, we develop and characterize such a model through empirical data recorded on a racing track, and then implement it on a racing wheelchair simulator with a haptic controller. Propelling on this simulator proved to be somewhat less challenging than real-life conditions, with a measured resistance force approximately 5 N lower than during real propulsion conditions. However, the resistance expectedly increased as simulated face wind increased. These results show a promising avenue for racing wheelchair athletes, both for training and assessing/correcting their biomechanics.

1 INTRODUCTION

Wheelchair sports have gained recognition for their positive impact on enhancing power, improving quality of life, increasing social participation, and reducing medical complications (Slater & Meade, 2004). However, a notable percentage of individuals who rely on manual wheelchairs for daily mobility, ranging from 30% to 73%, experience musculoskeletal disorders (MSDs) and shoulder or wrist pain due to repetitive loading during propulsion (Boninger et al., 2002; Finley & Rodgers, 2004). The risk of developing MSDs is even higher in wheelchair sports compared to regular wheelchair use, as the shoulder endures increased strain (Finley & Rodgers, 2004; Slater & Meade, 2004). Preserving musculoskeletal integrity is crucial for manual wheelchair users to maintain an active lifestyle, underscoring the importance of targeted sports training to mitigate the elevated risk of MSDs.

In comparison to other wheelchair sports such as basketball, tennis, or cycling, wheelchair racing is associated with a higher incidence of injuries (Roussot, 2014; Taylor & Williams, 1995). Thus, monitoring propulsion and studying its biomechanics holds significant importance in improving users' health. However, due to the limited availability of measuring instruments, the biomechanics of wheelchair racing remain understudied. To overcome the challenges of measuring and controlling various propulsion parameters in real-world settings, the use of in-laboratory devices, called simulators, becomes essential. These devices simulate wheelchair propulsion in a controlled and safe environment, enabling the measurement of different propulsion-related parameters and facilitating proper and safe propulsion training for users (Arlati et al., 2020; MacGillivray et al., 2020).

To ensure that research findings apply to real-life conditions, laboratory experiments must employ instruments that accurately replicate realistic dynamics (Vanlandewijck et al., 2001). In the case of stationary devices, it is crucial to model the non-linear relationship between wheelchair speed and resistance force. In wheelchair racing, this force comprises two primary components: 1) a constant and viscous component influenced by factors such as track hardness, tire pressure, wheel size, and the normal force exerted on the ground; and 2) a

Bayat, A. and Chénier, F.
Modelling Drag Forces on a Wheelchair Racing Simulator.
DOI: 10.5220/0012223300003587
In *Proceedings of the 11th International Conference on Sport Sciences Research and Technology Support (icSPORTS 2023)*, pages 187-193
ISBN: 978-989-758-673-6; ISSN: 2184-3201

component that is proportional to the square of the wheelchair velocity relative to the air, considering factors such as athlete's body position, aerodynamic profile, and air density (Barbosa et al., 2016; van der Woude et al., 2001). However, stationary devices on the market (e.g. Invacare Corp., Revolution Sports Inc.), employ mechanical rollers to support the rear wheels of racing wheelchairs and fail to replicate the intricate non-linear relationship between wheelchair speed, rolling resistance, and air resistance.

To address these challenges, we first modelled the relationship between total drag force and airspeed using empirical data, in order to accurately model propulsion on a stationary simulator with greater realism. Then, building upon the previous work of Chénier et al. (2014), we developed a wheelchair racing simulator that aims to accurately reproduce this non-linear resistance force, so that our system provides users with realistic feedback during propulsion, enhancing the overall simulation experience. The aim of this communication is to present our methodological development and compare the propulsion forces between real and simulated conditions.

2 METHODS

This study is composed of two phases. In the first phase, the equation relating the total resistance force and speed is developed and characterized using propulsion data from two wheelchair racing athletes on a racing track. In the second phase, this equation is implemented on the simulator and the ability of the simulator to reproduce this equation is tested with a wheelchair racing athlete.

2.1 Phase 1. Racing Wheelchair Dynamic Equations

The simulator needs a dynamic model of the racing wheelchair to be implemented on it. This model is expressed by:

$$F_{\text{propulsion}} - F_{\text{drag}} = ma \quad (1)$$

where $F_{\text{propulsion}}$ is the resulting linear force from the propulsive moments applied by the user on the pushrims that moves the wheelchair forward; F_{drag} is the force applied by the environment on the wheelchair/athlete to prevent its movement; m is the mass of the wheelchair/athlete, and a is the wheelchair acceleration. The drag force is modelled as:

$$F_{\text{drag}} = \mu_0 mg + \mu_1 mg v_{\text{wheelchair}} + \mu_2 (v_{\text{wheelchair}} + v_{\text{wind}})^2 \quad (2)$$

where μ_0 and μ_1 are the constant and viscous terms of the rolling resistance, and μ_2 is the air drag coefficient, proportional to the square of the difference between the wheelchair speed and the tail wind speed.

To characterize this equation, a first experiment took place on the Ben-Leduc 400m exterior racing track of Marcel-Laurin Park, Montreal, CA. Two wheelchair racing athletes were recruited for a study on the characterization of drag forces during racing wheelchair propulsion: 1) male, right-handed, cerebral palsy, T34 classification; 2) female, right-handed, double tibial amputee, T54 classification. They gave their informed consent, and the project was approved by the ethics committee of Université du Québec à Montréal, #CIEREH 2022–4098. They used their own racing wheelchair, where we replaced one rear wheel with an instrumented racing wheel similar to the one described in Chénier et al. (2021). This instrumented wheel records the propulsive forces and moments at a sampling rate of 2500 Hz. We weighed the instrumented wheelchair and athlete using 3 portable scales placed under each wheel.

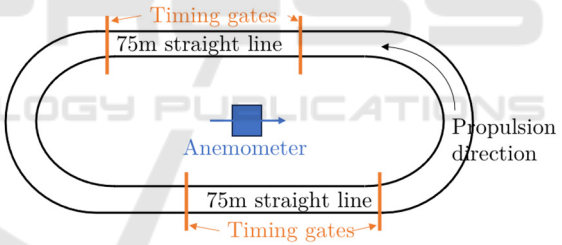

Figure 1: Racing track setup for determining the coefficients of the dynamic equation.

The athletes were asked to propel at different constant speeds of 14 to 20 km/h, controlled using a bicycle computer. The pushrim moments were measured using the instrumented wheel, which was synchronized to timing gates delimiting two 75m straight line zones as pictured in Fig. 1. Four measurements per speed were done, with the instrumented wheel installed on both sides. The tail wind speed v_{wind} was measured continually using an anemometer (PCE VA-20). Since $ma = 0$ at a constant speed, the total drag resistance F_{drag} was measured using the instrumented wheel using $F_{\text{drag}} = F_{\text{propulsion}}$. Due to assumed symmetry, $F_{\text{propulsion}} = 2M_{\text{propulsion}}/r_{\text{wheel}}$ where r_{wheel} is the radius of the rear wheel. This means that the

coefficients μ_0, μ_1 and μ_2 can be characterized by a least square optimization using the following equation:

$$\frac{2M_{\text{propulsion}}}{r_{\text{wheel}}} = \mu_0 mg + \mu_1 mg v_{\text{wheelchair}} + \mu_2 (v_{\text{wheelchair}} + v_{\text{wind}})^2 \quad (3)$$

with $M_{\text{propulsion}}$ being measured by the instrumented wheel, $v_{\text{wheelchair}}$ by the timing gates, and v_{wind} by the anemometer.

All 75-meter bouts were segmented using the timing gates. Then, to compensate for inertial forces due to anteroposterior body movement, only complete propulsion cycles were processed: for each bout, $M_{\text{propulsion}}$ was cut from the start of the first push up to the start of the last push and was averaged over this span.

The difference of $M_{\text{propulsion}}$ between both sides (trials with the instrumented wheel on the left vs. right) was 0.9 ± 3.7 Nm. There seems to be no side bias, which suggests that F_{drag} can effectively be estimated using only one wheel. Characterizing Eq. (3) yielded $\mu_0 = 0.00599$, $\mu_1 = 0.000785$ and $\mu_2 = 1.0187$, for a coefficient of determination of $R^2 = 0.606$.

2.2 Phase 2. Racing Wheelchair Simulator

Fig. 2 shows the racing wheelchair simulator, including both the roller and the racing wheelchair. The wheelchair's rear wheels sit on one roller that is controlled by a 120-volt brushless servomotor and drive.

Figure 2: UQAM Racing Wheelchair Simulator.

A force sensor is installed into the wheelchair supports that hold the wheelchair in place, as seen in Fig.3. By its location, it captures all the anteroposterior forces between the simulator and the wheelchair, including the inertial forces due to body movements.

Real-time information from the force sensor is fed to an admittance control loop using a real-time computer (SpeedGoat). The admittance control is a category of haptic controllers that controls the relationship between force and speed. In this controller, the input is the force and the controller regulates the speed as dictated by the dynamic equation to simulate (Cavenago et al., 2018). This control system was chosen for the wheelchair racing simulator as it is suited for controlling systems with high inertia (Chenier et al., 2014; Keemink et al., 2018). Fig. 4 shows the block diagram for an admittance control block. Both the dynamic model and speed controller (a proportional-integral—PI controller) were implemented using Simulink Real-Time on the SpeedGoat computer.

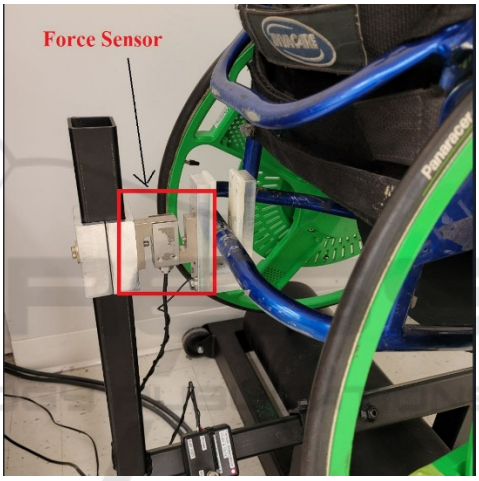

Figure 3: Force Sensor Location.

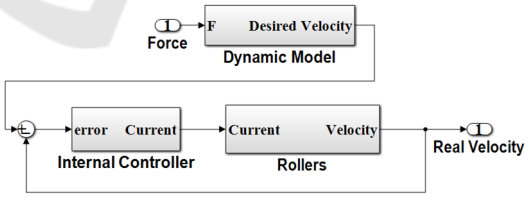

Figure 4: Block Diagram of Admittance Control.

The Simulink implementation of this simulator is a novel modular structure where each part of the system (e.g., force sensor input, dynamic model, speed controller) is a separate block designed for code reuse, and that includes its own unit test procedure. This structure helps to easily add blocks or iteratively enhance the system, avoiding redesigns. It also uses predefined configuration settings that will help researchers from other labs to integrate this work into other wheelchair simulators,

using different versions of MATLAB/Simulink. Fig. 5 and Fig. 6 show the block diagram of the speed controller and dynamic model respectively.

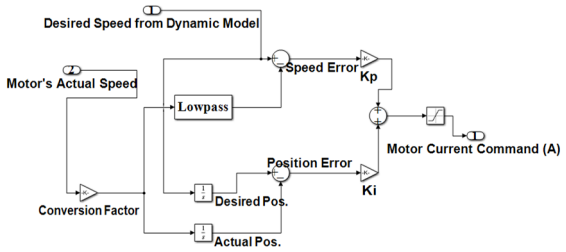

Figure 5: Block Diagram of Speed Controller.

In the speed controller (Fig. 5), the conversion factor for the motor drive is defined based on the radius ratio of the wheel, roller, and motor shaft. This speed signal is then filtered by a low-pass Bessel filter of order 2 with a cutoff frequency of 20 Hz. The gains for the PI controller were defined based on the Ziegler method, and then modified by trial and error, for final values of Kp = 7 and Ki = 5.

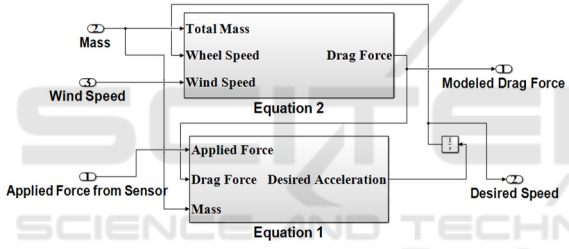

Figure 6: Block Diagram of Racing Wheelchair Dynamic Model.

Equations 1 and 2 were implemented inside the dynamic model (Fig. 6), which gives two outputs: the modelled drag force is based on Eq. (2), and it allows calculating a desired speed based on Eq. (1).

After calibrating the system (essentially removing the force sensor offset), the simulated parameters such as the wind speed can be sent in real time to the simulator, allowing for the change of the propulsion conditions inside the same propulsion acquisition.

2.3 Experimental Test of the Racing Simulator

Participant 2 of Phase 1 was re-invited for a test experiment of the UQAM Racing Wheelchair Simulator. His own racing wheelchair was affixed to the simulator and the right wheel was replaced by the instrumented wheel.

Table 1: Steady-state propulsion on the simulator.

Task	Wheelchair speed (km/h)	Wind speed (m/s)
1	10	1
2	10	0
3	10	-1
Rest		
4	12	1
5	12	0
6	12	-1
Rest		
7	14	1
8	14	0
9	14	-1

The athlete propelled on the simulator in three blocks of constant speed, each segmented into three wind speeds (no wind, 1 m/s tail wind, 1 m/s face wind), as shown in Table 1 where a positive wind speed value is a tail wind. He propelled for each segment for the time equivalent to 75 m and had a rest between blocks. Speed was controlled using a bicycle computer.

After the propulsion, he answered a few quick questions about his perception of the realism and usefulness of the simulator.

2.3.1 Measured Parameters and Analysis

To verify the ability of the speed controller to match the desired speed, we compared the desired speed to the real speed.

Then, to verify the ability of the simulator to match the desired drag force, we used the propulsive moment measured by the instrumented wheel ($M_{propulsion}$) to calculate the average measured drag force F_{drag} using the same method as in phase one. The F_{drag}(modelled) is the output of Equation 2 which was implemented in Dynamic Model Block. For each task of Table 1, the average measured drag force was compared to the average drag force modelled by the simulator.

3 RESULTS

Fig. 7 presents a comparison of the desired and real speed in m/s for a few pushes during task 5 (12 km/h, no wind) as an example. Overall, the RMS of the error was of 0.0413 m/s for the controller.

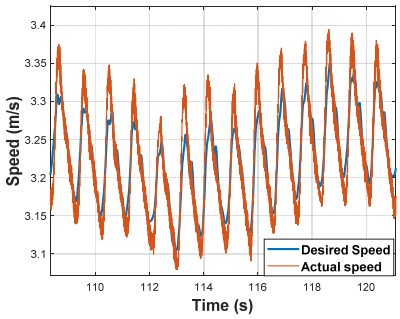

Figure 7: Desired and Real speed during a few pushes at 12 km/h block and 0 m/s wind speed segment.

Fig. 8 shows the modelled and measured drag force during the same pushes as Fig. 7.

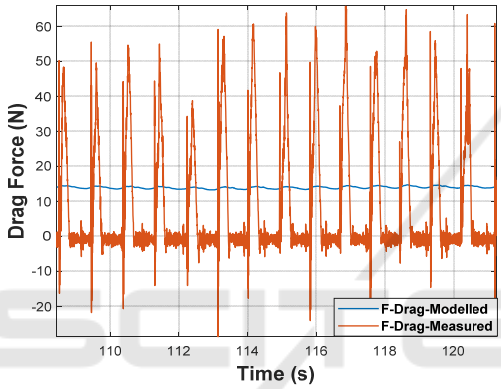

Figure 8: Values of modelled and measured F_{drag} during a few pushes at 12 km/h block and 0 m/s wind speed segment.

Table 2 compares average values of modelled and measured forces for all propulsion tasks during the complete cycles with constant speed. As we observe, the average value of drag force that the user really overcame (measured F_{drag}) was lower than the one modelled by Eq. (2) (modelled F_{drag}) by about 4.9 N, which suggests that it was easier to propel on the simulator than in real conditions. The mean value and standard deviation of these two forces show that their difference is only a constant value.

Table 2: Average values of modelled and measured drag force in different propulsion conditions on the simulator.

	Wind speed (m/s)	Avg. Model'd F_{drag} (N)	Avg. Meas. F_{drag} (N)	Diff. (N)
Block1 10 km/h	1	6.8	2.2	-4.6
	0	11.5	6.9	-4.6
	-1	17.7	12.6	-5.1
Block2 12 km/h	1	8.2	3.4	-4.8
	0	13.8	8.1	-5.7
	-1	21.2	16.2	-5.0
Block3 14 km/h	1	10.2	4.7	-5.5
	0	16.7	11	-5.7
	-1	23.1	20.3	-2.8
Mean		14.4	9.5	-4.9
Std.		5.7	6.1	0.9

4 DISCUSSION

Propelling on the simulator proved to be easier for the athlete than intended. This discrepancy between the modelled and measured drag forces may be attributed to the lag in the controller's response to rapid changes. The controller fails to follow the desired speed during rapid transitions, as depicted in Fig. 7. Consequently, the wheel may accelerate faster than it should during the first portion of the push, resulting in a lower resistance.

This finding is particularly intriguing when we compare this simulator with the LIO simulator (Chenier et al., 2014) that uses a similar admittance-based controller. However, in the LIO simulator, the input force is measured by two instrumented wheels instead of a force sensor at the rear of the wheelchair. As a result of reading the external force directly applied to the wheel, the LIO simulator's controller uses this information in a feed-forward configuration to directly compensate for the perturbation applied by the user. In contrast, the current simulator substitutes the instrumented wheel with a force sensor, following the configuration in Pizzaro-Chong (2020). This modification enhances the affordability, both in terms of cost and time, as the athletes do not need to change their wheels for instrumented wheels on the simulator. Furthermore, this change facilitates the capture of all forces, including the inertial forces due to body movement, which may enhance the realism of the simulator (Chenier et al., 2016). However, the drawback of using the force sensor is that we could not implement such a feedforward, as we do not measure the force applied on the pushrims by the user. Consequently, the controller could not react as fast to these external perturbations. This is especially important for a racing wheelchair simulator, where the athletes apply high forces, at high speed, during short amounts of time.

To address this limitation, we propose including a physical inertia such as a flywheel in a future iteration of the simulator, in addition to the electronic inertia provided by our admittance controller. This additional physical inertia will compensate instantly for most of the perturbation exerted by the user while letting the controller reach

a steady state using a similar proportional-integral architecture.

Overall, the athlete's perception of the experiment was highly positive. He expressed great satisfaction with the simulation, noting its similarity to real conditions, where changes in wind speed affect the sensation of resistance. From a training aspect, the advantage of the simulator lies in providing a controlled training environment without the challenges faced when practising outdoors, particularly in colder climates where exterior racing tracks are unavailable during winter. However, the athlete did mention a slight disparity in the perceived amount of resistance compared to overground conditions, which aligns with the observations from the results.

The primary limitation of this study is the restricted speed range in which the racing wheelchair was evaluated. To comprehensively assess its performance, higher speeds should be investigated. However, due to the availability of only one motor that lacked sufficient strength to accommodate higher desired speeds, this objective could not be achieved within the scope of this study. Additionally, the participant pool was limited to a single individual, which restricted the ability to fully comprehend the simulator's strengths and weaknesses. Including a larger number of participants would provide valuable insights in this regard.

Future studies on the validation of this simulator should investigate not only the drag mean force, but other biomechanical variables such as instantaneous force, power, and speed on both real and simulated tracks. This comparison will establish the simulator's potential as a valuable tool to evaluate the biomechanics of wheelchair racing, and eventually as a better training tool for athletes.

5 CONCLUSION

The availability of a dependable stationary device for racing wheelchair athletes, facilitating ecological biomechanical measurement and training, is of paramount importance. The simulator presented in this work, along with the suggested dynamic model, holds promise in serving this purpose. By adjusting the resistance experienced by athletes according to wind speed and their applied force, a more realistic biomechanical assessment and training experience can be achieved.

REFERENCES

Arlati, S., Colombo, V., Ferrigno, G., Sacchetti, R., & Sacco, M. (2020). Virtual reality-based wheelchair simulators: A scoping review. *Assistive Technology*, *32*(6), 294—305. https://doi.org/10.1080/10400435.2018.1553079

Barbosa, T. M., Forte, P., Estrela, J. E., & Coelho, E. (2016). Analysis of the Aerodynamics by Experimental Testing of an Elite Wheelchair Sprinter. *Procedia Engineering*, *147*, 2—6. https://doi.org/10.1016/j.proeng.2016.06.180

Boninger, M. L., Souza, A. L., Cooper, R. A., Fitzgerald, S. G., Koontz, A. M., & Fay, B. T. (2002). Propulsion patterns and pushrim biomechanics in manual wheelchair propulsion. *Archives of Physical Medicine and Rehabilitation*, *83*(5), 718–723. https://doi.org/10.1053/apmr.2002.32455

Cavenago, F., Voli, L., & Massari, M. (2018). Adaptive Hybrid System Framework for Unified Impedance and Admittance Control. *Journal of Intelligent & Robotic Systems*, *91*(3–4), 569–581. https://doi.org/10.1007/s10846-017-0732-1

Chenier, F., Bigras, P., & Aissaoui, R. (2014). A New Wheelchair Ergometer Designed as an Admittance-Controlled Haptic Robot. *IEEE/ASME Transactions on Mechatronics*, *19*(1), 321—328. https://doi.org/10.1109/TMECH.2012.2235079

Chenier, F., Gagnon, D. H., Blouin, M., & Aissaoui, R. (2016). A Simplified Upper-Body Model to Improve the External Validity of Wheelchair Simulators. *IEEE/ASME Transactions on Mechatronics*, *21*(3), 1641–1649. https://doi.org/10.1109/TMECH.2016.2527240

Chénier, F., Pelland-Leblanc, J.-P., Parrinello, A., Marquis, E., & Rancourt, D. (2021). A high sample rate, wireless instrumented wheel for measuring 3D pushrim kinetics of a racing wheelchair. *Medical Engineering & Physics*, *87*, 30–37. https://doi.org/10.1016/j.medengphy.2020.11.008

Finley, M. A., & Rodgers, M. M. (2004). Prevalence and identification of shoulder pathology in athletic and nonathletic wheelchair users with shoulder pain: A pilot study. *Journal of Rehabilitation Research and Development*, *41*(3B), 395—402. https://doi.org/10.1682/jrrd.2003.02.0022

Keemink, A. Q., van der Kooij, H., & Stienen, A. H. (2018). Admittance control for physical human—robot interaction. *The International Journal of Robotics Research*, *37*(11), 1421—1444. https://doi.org/10.1177/0278364918768950

MacGillivray, M. K., Eng, J. J., Dean, E., & Sawatzky, B. J. (2020). Effects of Motor Skill-Based Training on Wheelchair Propulsion Biomechanics in Older Adults: A Randomized Controlled Trial. *Archives of Physical Medicine and Rehabilitation*, *101*(1), 1–10. https://doi.org/10.1016/j.apmr.2019.07.017

Pizarro-Chong, A. D. (2020). *Development and Validation of the Control Loops for the Haptic Interfaces of a Standard Manual Wheelchair Simulator*. 177.

Richter, W. M., Kwarciak, A. M., Guo, L., & Turner, J. T. (2011). Effects of Single-Variable Biofeedback on Wheelchair Handrim Biomechanics. *Archives of Physical Medicine and Rehabilitation*, *92*(4), 572–577. https://doi.org/10.1016/j.apmr.2010.11.001

Roussot, M. (2014). *Upper limb injuries in athletes participating at the London 2012 Paralympic Games* [Master Thesis, University of Cape Town]. https://open.uct.ac.za/handle/11427/13312

Slater, D., & Meade, M. A. (2004). Participation in recreation and sports for persons with spinal cord injury: Review and recommendations. *NeuroRehabilitation*, *19*(2), 121–129.

Taylor, D., & Williams, T. (1995). Sports injuries in athletes with disabilities: Wheelchair racing. *Paraplegia*, *33*(5), 296—299. https://doi.org/10.1038/sc.1995.67

van der Woude, L. H. V., Veeger, H. E. J., Dallmeijer, A. J., Janssen, T. W. J., & Rozendaal, L. A. (2001). Biomechanics and physiology in active manual wheelchair propulsion. *Medical Engineering & Physics*, *23*(10), 713–733. https://doi.org/10.1016/S 1350-4533(01)00083-2

Vanlandewijck, Y., Theisen, D., & Daly, D. (2001). Wheelchair Propulsion Biomechanics: Implications for Wheelchair Sports. *Sports Medicine*, *31*(5), 339–367. https://doi.org/10.2165/00007256-200131050-00005